Exploring Lignification Complexity in Plant Cell Walls with Airyscan Super-resolution Microscopy and Bioorthogonal Chemistry

Clemence Simon, Oriane Morel, Godfrey Neutelings, Fabien Baldacci-Cresp, Marie Baucher, Corentin Spriet, Christophe Biot, Simon Hawkins, Cedric Lion

ACS Partner Journal

CHEMICAL & BIOMEDICAL IMAGING

pubs.acs.org/ChemBioImaging

Article

Exploring Lignification Complexity in Plant Cell Walls with Airyscan Super-resolution Microscopy and Bioorthogonal Chemistry

Clémence Simon, Oriane Morel, Godfrey Neutelings, Fabien Baldacci-Cresp, Marie Baucher, Corentin Spriet, Christophe Biot, Simon Hawkins, and Cédric Lion*

Cite This: *Chem. Biomed. Imaging* 2023, 1, 479–487

Read Online

ACCESS | Metrics & More | Article Recommendations | Supporting Information

ABSTRACT: In this paper, we present the use of multiplex click/bioorthogonal chemistry combined with super-resolution Airyscan microscopy to track biomolecules in living systems with a focus on studying lignin formation in plant cell walls. While laser scanning confocal microscopy (LSCM) provided insights into the tissue-scale dynamics of lignin formation and distribution in our previous reports, its limited resolution precluded an in-depth analysis of lignin composition at the unique cell wall or substructure level. To overcome this limitation, we explored the use of Airyscan microscopy, which, among the super-resolution techniques available, offers an optimal balance between performance, cost, accessibility, and ease of implementation. Our study demonstrates that a triple labeling strategy using copper-catalyzed azide−alkyne cycloaddition (CuAAC), strain-promoted azide−alkyne cycloaddition (SPAAC), and inverse electronic-demand Diels−Alder cycloaddition (IEDDA) to label modified lignin metabolic precursors can be combined with Airyscan microscopy to reveal the zones of active lignification at the single cell level with improved sensitivity and resolution. This approach enables insights into the lignin composition in wall substructures, such as pits or in wall layers that are otherwise not distinguishable by classical LSCM. Our work emphasizes the importance of studying lignin formation in plant cell walls and demonstrates the potential of combining bioorthogonal chemistry and super-resolution microscopy techniques for studying biomolecules in living systems.

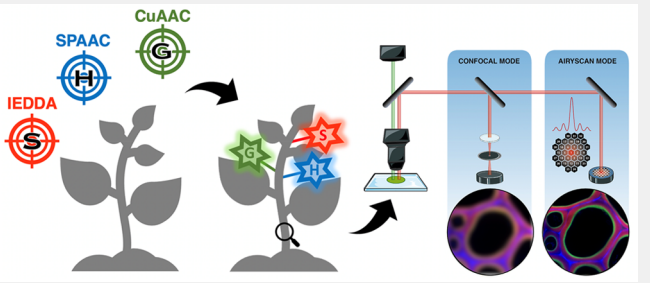

KEYWORDS: *Plant chemical biology, click chemistry, bioorthogonal chemistry, super-resolution bioimaging, lignin*

INTRODUCTION

In 2022, the Nobel Prize in Chemistry was awarded to Meldal and Sharpless for their pioneering work in the development of click chemistry and to Bertozzi for her contributions to bioorthogonal chemistry, a class of reactions that occur in biological environments without interfering with endogenous processes.[1,2] The typical approach involves a two-step strategy, in which a synthetic analogue of the metabolite of interest (bearing a small, nontoxic, and biologically inert tag, such as an azide or alkyne group) is first incorporated into a living cell or organism by hijacking its enzymatic machinery. After metabolic incorporation, a detectable molecular probe (*e.g.*, a fluorochrome for bioimaging purposes) is then covalently and specifically conjugated to the introduced reporter tags through a chemoselective and biocompatible reaction. Coined bioorthogonal reactions, these ligations often fullfill the criteria of click chemistry as they are high-yielding and exhibit fast kinetics,[3] and mostly belong to the cycloaddition family. Bioorthogonal chemistry has been applied successfully to diverse biological models over the past 20 years[4−6] and has greatly facilitated *in vivo*, *ex vivo*, and *in situ* studies of the main classes of biomolecules[7] such as glycans,[8,9] lipids,[10] nucleic acids,[11] and proteins exploiting a wide range of bioanalytical and bioimaging readout techniques.[12,13] Although many notable examples have been described in mammalian living systems,[14,15] there are surprisingly few reports in plants,[16−22] despite the fact that they represent 82% of all living matter on earth and make up the first economic resource in terms of nutrition, renewable materials and renewable energies. Lignin is one of the main constituents of plant cell walls, with cellulose. This complex phenolic biopolymer is crucial for vascular transport and mechanical support,[23] and contributes to plant resistance against abiotic stress and pathogens.[24] Considering its colossal economic impact on the industrial valorization of plant biomass, the importance of gaining further insight into the factors and mechanisms that regulate lignification processes in plants cannot be overstated in today's environmental context.

Received: April 19, 2023
Revised: June 9, 2023
Accepted: June 13, 2023
Published: July 6, 2023

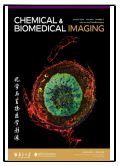

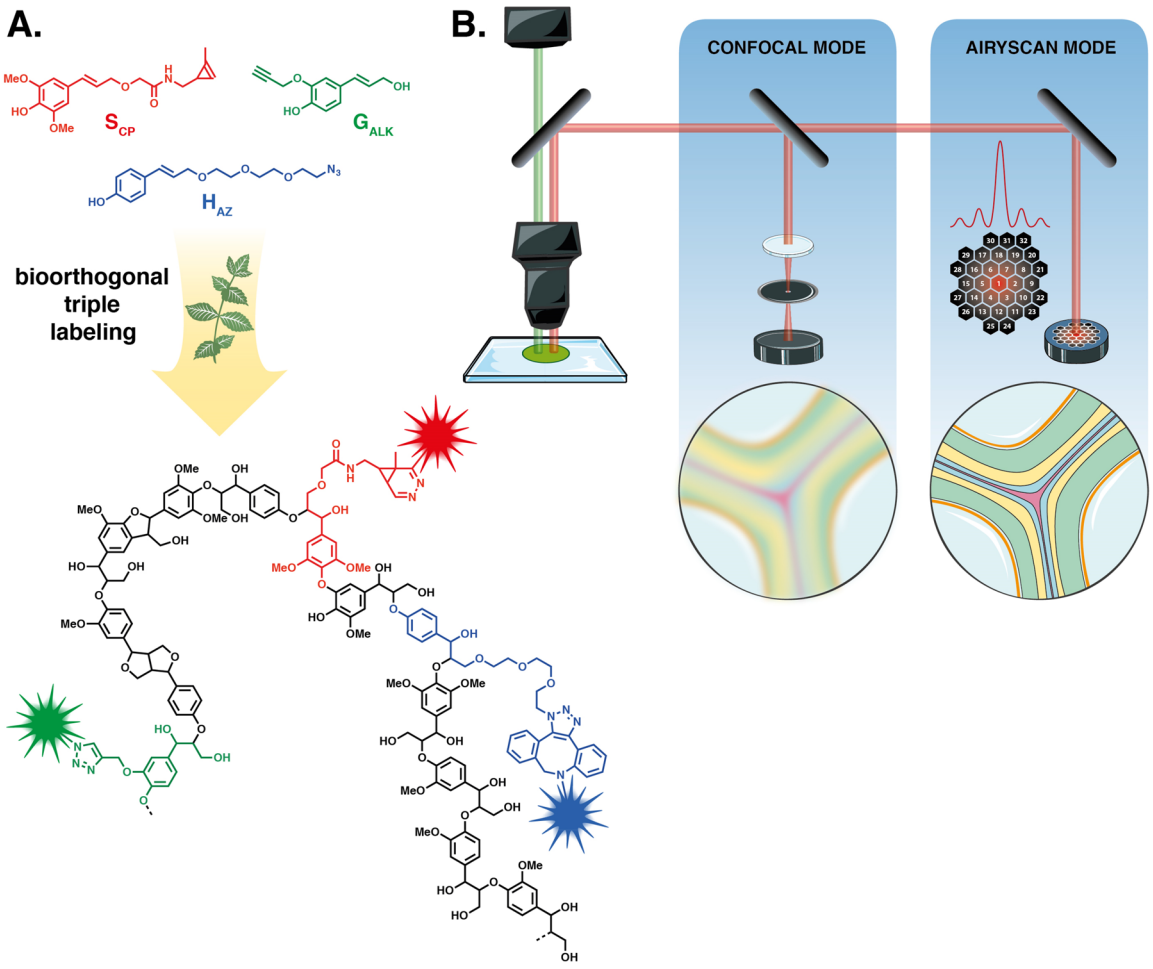

Figure 1. Overview of the bioorthogonal triple labeling strategy. (A) Chemical reporters S_{CP}, H_{AZ}, and G_{ALK} are tagged analogs of the monolignols sinapyl alcohol (S), *p*-coumaryl alcohol (H), and coniferyl alcohol (G), respectively. They are first metabolically incorporated into growing lignin polymers of the cell walls by exogenous feeding. (i) Tetrazine-, (ii) cyclooctyne-, and (iii) azide-functionalized fluorescent probes are then specifically ligated to the incorporated reporters (i) S_{CP}, (ii) H_{AZ}, and (iii) G_{ALK} by three successive bioorthogonal reactions: (i) IEDDA, (ii) SPAAC, and (iii) CuAAC. This allows the specific localization of all three reporters independently in the same sample. (B) Illustration of the resolution gain in cell wall visualization: comparison of confocal mode versus Airyscan mode.

In recent reports, we described bioorthogonal labeling methods utilizing laser-scanning confocal microscopy (LSCM) to visualize the spatiotemporal dynamics of lignin formation and distribution in cell walls, as well as that of other structural polysaccharides (Figure 1).[25,26,21] This allowed us to track active lignification zones in various tissues of plants of scientific and/or economic interest such as flax, *Arabidopsis*, poplar, or tobacco. LSCM is a widely used and powerful imaging technique that provides optical sectioning capabilities and improved resolution compared to wide-field microscopy,[27] and this technique is used routinely to acquire imaging data following bioorthogonal labeling. However, due to Abbe's law, its lateral resolution remains limited to roughly 0.25 μm in practice for most real biological samples, even when high-end objectives are employed. This diffraction barrier hinders the full potential of optical microscopy for the in-depth study of complex biological structures, such as plant cell walls. To gain deeper insights into the intricate mechanisms governing the formation of specific substructures, it is essential to combine such labeling strategies with technologies that achieve a higher resolution.

Until recently, electron microscopy (EM) and atomic force microscopy (AFM) were the techniques of choice when requiring very high spatial resolution. However, EM and AFM cannot use the advantages offered by photonic microscopy, such as multiplex labeling of specific biomolecules for dynamic studies in living samples. With the advent of super-resolution microscopy, a range of techniques is now available to address these challenges. Stimulated emission depletion microscopy (STED),[28] photoactivated localization microscopy (PALM),[29,30] and stochastic optical reconstruction microscopy (STORM)[31,32] have revolutionized optical nanoimaging. These advancements were so significant that they were honored with the 2014 Nobel Prize in Chemistry, ushering in a new era for bioimaging.[33]

However, implementing STED, PALM, and STORM techniques can be extremely challenging, and even today, they usually require the convergence of several favorable conditions in order to be applied successfully. For example, STED microscopy requires very complex and costly instrumentation that is not commonly available in most laboratories,[34] and its increased resolution comes at the cost of lower sensitivity as it relies on selective de-excitation of fluorophores by a depletion laser to achieve super-resolution. On the other hand, single molecule localization imaging by PALM and STORM technologies has the advantage of

https://doi.org/10.1021/cbmi.3c00052
Chem. Biomed. Imaging 2023, 1, 479−487

increased sensitivity *and* resolution, but their use is very time-demanding and complex in terms of sample preparation and experiment optimization, requiring highly specialized expertise. Furthermore, the use of adapted fluorophores is also necessary, but the options for available photoswitchable molecular tools are limited in number. Time-resolution is also much lower, and such approaches are not well suited to live cell imaging because of the use of high-power density and lengthy acquisition times.[32] Thus, these most advanced super-resolution technologies are not readily accessible to nonspecialist users for routine read-out experiments, and there is a need to find a balance between resolution, cost, ease of use, and speed, both regarding sample preparation and data acquisition.[35]

In light of these considerations, we thus shifted our focus toward the recently developed Airyscan technology, which employs a 32-channel gallium arsenide phosphide photomultiplier tube (GaAsP-PMT) detector. Airyscan indeed offers a compelling combination of advantages from both LSCM and super-resolution techniques, including affordability, user-friendliness, no requirement for intricate alignment between channels, the ability to utilize a diverse range of chemically stable, commercially available fluorophores with high quantum yields that span the entire spectrum, and rapid acquisition rates. Additionally, Airyscan provides a significantly higher sensitivity than LSCM, further enhancing its appeal as a potential solution for advanced imaging needs.[36,37]

The application of super-resolution imaging techniques to the study of plants is a relatively unexplored area, with only a handful of reports in the scientific literature.[38,39] Furthermore, studies focusing specifically on the analysis of plant cell walls are scarce, despite the clear advantages that enhanced spatial resolution could offer in this field.[40] STORM was employed to observe cellulose microfibrils in a report,[41] and to study the role of pectins in lobe formation in *Arabidopsis* pavement cells in another.[42] Concerning lignin, its cell wall distribution was investigated in 2018 by STED microscopy combined with polyethylene glycol-rhodamine (PEG-R) conjugates,[43] then in 2022 with super resolution radial fluctuation (SRRF) microscopy associated with lignin conventional stains or autofluorescence.[44] To the best of our knowledge, the latter are the only two reported attempts at super-resolution microscopy on the topic of lignin.

While it is well established that the amount and composition of lignin found in the plant cell wall vary depending upon a number of factors (*e.g.*, species, tissue/cell-type, cell wall layer/zone), the underlying physical and biological reasons for such differences are still not completely understood, especially at the cell wall level. Several hypotheses can be proposed to explain this, including differential transcriptional regulation of the monolignol biosynthesis pathway and regulation of the quantity/localization of different cell wall monolignol oxidizing enzymes (*e.g.*, peroxidases, laccases) as well as the effect of variability in the structure of the polysaccharide matrix within which lignification occurs. The ability to characterize lignification dynamics with improved spatial resolution will contribute, in combination with other techniques, to a better understanding of the physical/biological reasons underlying the observed variability in cell wall lignin quantity/structure. Herein, we show that bioorthogonal chemistry can be combined with the use of turn-key super-resolution Airyscan microscopes to study the dynamics of lignin formation in plant cell walls at a single cell wall layer or substructure scale. Using three monolignol reporters, we implement a multiplexed metabolic lignin labeling strategy that allows the precise observation of individual cell wall layers and of lignified depressions of the secondary cell walls called pits, and their ability to differentially incorporate the three units that compose lignin. The method is easy to use and only requires readily prepared lignin chemical reporters and commercially available, bright, inexpensive "clickable" fluorophores. It provides a significant increase in resolution, allowing much finer analyses of cell wall substructures and layers.

RESULTS AND DISCUSSION

Gaining a more profound understanding of lignification regulation and dynamics at the subcellular level necessitates the ability to distinguish between pre-existing lignin already present in the plant and the lignin being produced at a given time. This differentiation, which is necessary to accurately locate active lignification zones, cannot be achieved by using histochemical stains. In a recent report, we demonstrated the efficacy of a triple click-labeling strategy that utilizes chemical reporters to visualize the dynamic incorporation of H, G, and S monolignol analogs (termed H_{AZ}, G_{ALK}, and S_{CP}, respectively) into lignifying cell walls in plant tissues, which we adapted here with modifications on flax (*Linum usitatissimum*) and thale cress (*Arabidopsis thaliana*) (Figure 1A).[26] Three modified monolignol reporters S_{CP}, H_{AZ}, and G_{ALK} were thus synthesized in three-seven steps from the corresponding carboxylic acid (*i.e.*, sinapic acid, *p*-hydroxycoumaric acid, and ferulic acid, respectively; see Supporting Information for detailed procedures), each of them bearing a chemical reporter tag than can be reacted specifically with a molecular probe by bioorthogonal chemistry. After simultaneous metabolic incorporation of S_{CP}, H_{AZ} and G_{ALK} monolignol reporters into plant stem cross sections, the three main bioorthogonal click ligations were employed to specifically label each reactive handle. Methylcyclopropenyl tags introduced on sinapyl alcohol, corresponding to lignin S units, were labeled with a tetrazine-equipped fluorophore after inverse electronic demand Diels−Alder cycloaddition (IEDDA). Azido tags introduced on the modified *p*-hydroxycoumaryl alcohol (incorporated into lignin as H units) were specifically labeled with a cyclooctyne-functionalized fluorophore via a strain-promoted azide−alkyne cycloaddition (SPAAC). Finally, terminal alkynyl tags, introduced on coniferyl alcohol that leads to lignin G units, were labeled with a copper-catalyzed azide−alkyne cycloaddition (CuAAC). The specificity of each fluorophore and bioorthogonal reaction to its corresponding monolignol was validated by us in previous reports.[21,25,26]

Although this approach is of great interest, the resolution obtained with conventional confocal microscopy is limited (ca. 240−260 nm depending upon the fluorophore emission wavelength), thus restricting the amount of biologically relevant information that could potentially be obtained from the marking pattern. While it would have been possible to employ super-resolution techniques such as STORM, PALM, or STED that offer a far higher resolution (*e.g.*, up to 20 nm for STORM/PALM and up to 30 nm for STED are indicated by commercial microscopy companies), doing so would have necessitated a laborious and time-intensive phase of technical development and optimization. In this sense, the Airyscan technology represents an excellent compromise between classical LSCM and the most performing super-resolution techniques, being spatially (ca. 100−120 nm) and temporally more resolutive as well as more sensitive than LSCM, while

https://doi.org/10.1021/cbmi.3c00052
Chem. Biomed. Imaging 2023, 1, 479−487

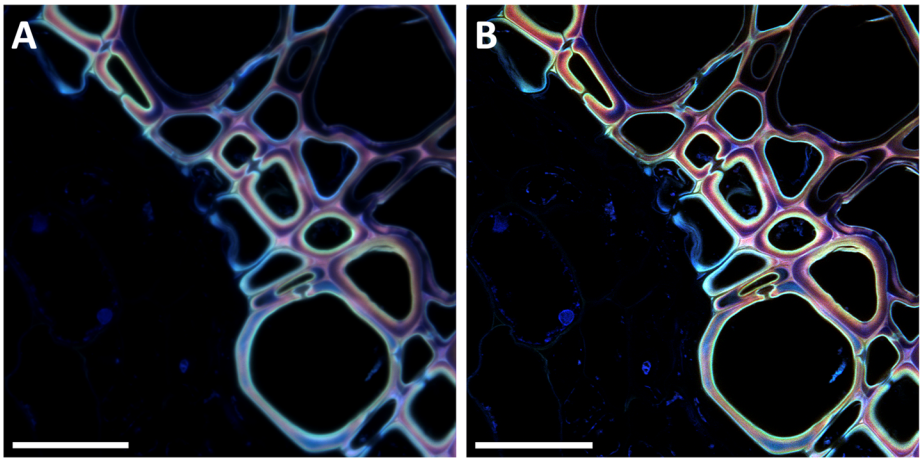

Figure 2. Airyscan vs conventional confocal laser scanning microscopy images. Merged channel images of flax stem xylem obtained with (A) conventional LSCM and (B) Airyscan super-resolution. Scale bar: 20 μm.

retaining the same low cost and capability for routine-based acquisition by nonspecialist users (Figure 1B). Turnkey systems that do not require highly specialized skills are now commercially available at a cost not far greater than that of a classical confocal microscope. Moreover, there is a wide choice of commercially available fluorescent probes functionalized with clickable moieties. All fluorophores are indeed suitable for Airyscan, facilitating transfer of the methodology from classical LSCM. In this instance, simple clickable rhodamines and cyanines were employed. The technology relies on the use of a specialized 32-channel GaAsP-PMT detector in which each of the 32 detector elements is organized in a compound-eye pattern and functions as a miniature 0.2 Airy Units (AU) pinhole, thus preserving spatial information *and* sensitivity. This detector combines the advantages of high resolution from imaging with a small pinhole and high photon collection efficiency from imaging with a large pinhole, which is not achievable by LSCM. Compared to Airyscan, a confocal microscope with a pinhole size of 0.2 AU would indeed detect less than 5% of the photon count, leading to a dramatic 95% decrease in the signal. Most LSCM setups are thus conventionally used with a 1.0 AU pinhole size. Moreover, the overall diameter of the Airyscan array is 1.25 AU, allowing the detection of 50% more light than conventional LSCM with a 1.0 AU pinhole. The 32 simultaneously acquired images are then processed and provide a 1.7× to 2.4× increase in *xyz* resolution combined with at least 4−8× improvement of the signal-to-noise ratio compared to equivalent LSCM acquisition.[45] Not only is Airyscan a more resolutive technology but it is also more sensitive, thus allowing detection of lesser amounts of reporter incorporation in smaller substructures of cell walls that are actively producing lignin. To show the advantages of this platform, we acquired classical LSCM and Airyscan images of plant cell walls in the same area of flax stem xylem (Figure 2) and of *Arabidopsis* interfascicular fibers and xylem (Figure S1).

While both techniques provide satisfying data to exploit our triple labeling method for dynamic studies of lignification (*e.g.*, identification of zones that are actively forming lignin at a given time, spatial specificity of different monolignol precursors during development), the Airyscan images exhibit significantly greater resolution, sharpness, and contrast, allowing the observation of smaller features than LSCM. The capacity to obtain more detailed and relevant biological information about the lignification process in flax xylem was confirmed by comparing fluorescence signal intensity profiles for the different reporters obtained on the same cell wall regions observed by standard LSCM or Airyscan. Conventional profiles obtained by LSCM enabled the identification of three main zones (zones 1−3) of reporter incorporation, despite the fact that different substructures (*i.e.*, middle lamella, primary cell wall, S1 and S2 secondary cell wall layers) are known to be present (Figure 3, panel A). In contrast, the profiles obtained using the Airyscan detector revealed a more complex pattern of reporter incorporation that more easily allows the different cell wall layers to be identified (Figure 3, panel B). Observation of both images and intensity profiles indicates that these different cell wall layers do not uniformly incorporate all of the different reporters to the same extent. While the incorporated H and G reporters show similar, but not identical, fluorescence intensity profiles for most of the cell wall layers, clear differences can be observed with the S reporter that appears to be preferentially incorporated in the $S2_Y$ and $S2_O$ layers compared to H and G. The capacity to more easily attribute reporter signal to different cell wall layers represents an important step toward understanding the spatial and temporal regulation of lignification in cell walls, thereby contributing to a better general understanding of developmental biology in plants.

As an example of how the combined triple click labeling and Airyscan super-resolution could be used to improve our knowledge of cell wall formation in plants, we used this approach to investigate more closely the process of lignification in the pit region of flax xylem and *Arabidopsis* interfascicular fibers. In plant cells, the plasma membrane is surrounded by a cell wall that confers mechanical support and protects the cell. Depending upon the nature of the wall, *e.g.*, primary vs secondary, cell-to-cell movement of water and other molecules is more or less regulated. In cells with thick secondary, often lignified, cell walls, discontinuities in the secondary cell wall structure known as pits play an important role in facilitating and regulating cell to cell movement. Such structures are particularly abundant in xylem tissues where they contribute to efficient water transport between different cell types.[46] Previous studies have indicated that the region of the cell wall immediately adjacent to the pit discontinuity is more heavily lignified than other regions of the cell wall more distant,[47,48] suggesting that increased mechanical resistance of

https://doi.org/10.1021/cbmi.3c00052
Chem. Biomed. Imaging 2023, 1, 479−487

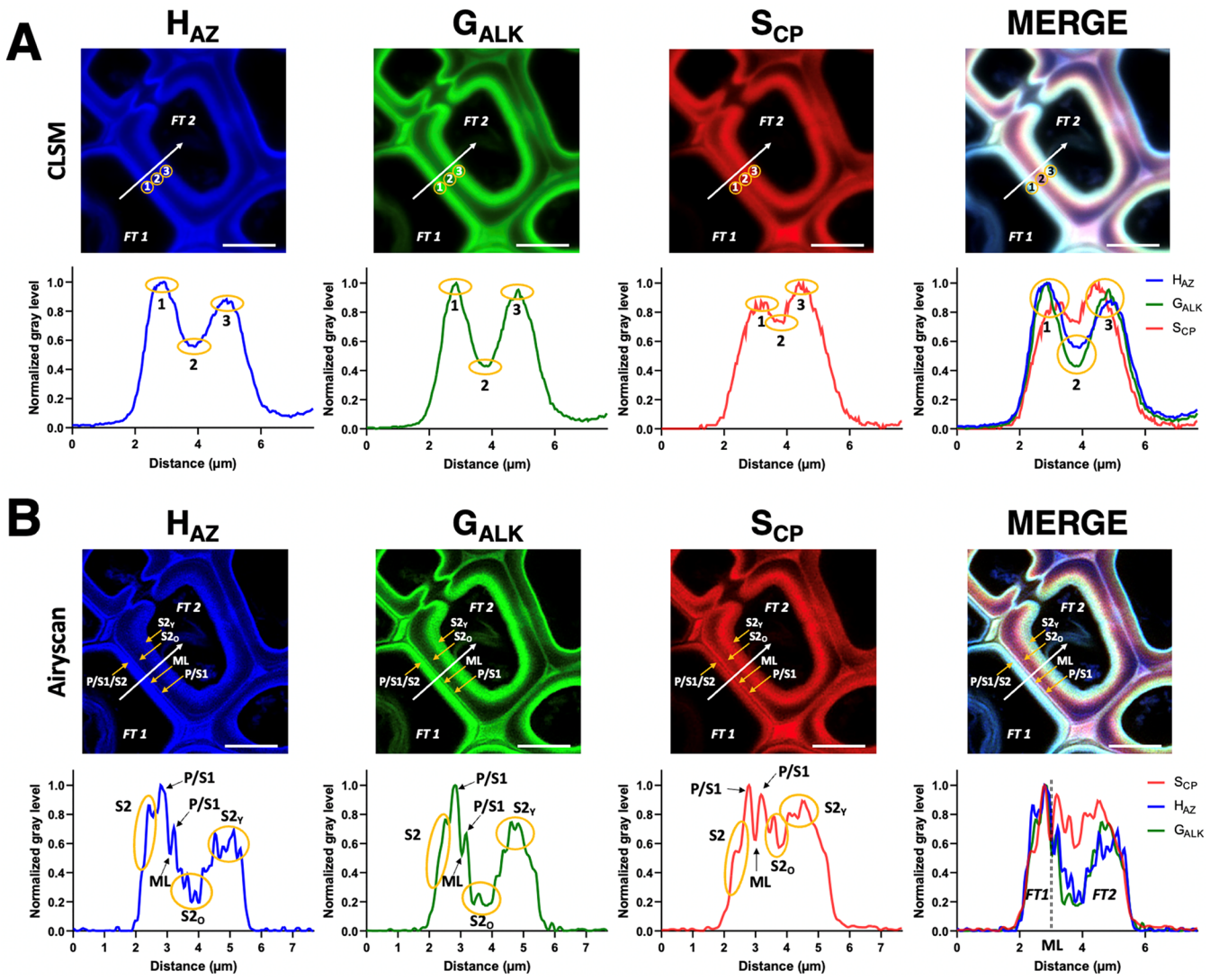

Figure 3. Airyscan vs conventional confocal microscopy images and probe intensity profiles in flax xylem fiber-tracheids. (A, B) Single channel images (H_{AZ}, G_{ALK}, S_{CP}) and merge channel image together with corresponding probe intensity profiles obtained with (A) conventional confocal microscopy vs (B) Airyscan microscopy. White arrows represent the vectors used for probe intensity profiles. FT 1 = fiber-tracheid 1 (younger cell), FT 2 = fiber-tracheid 2 (older cell), circles 1−3 = cell wall zones 1−3 identified by conventional confocal microscopy, ML = middle lamella, *P* = primary cell wall, S1 = secondary cell wall S1 layer, $S2_Y$ = younger region of secondary cell wall S2 layer, $S2_O$ = older region of secondary cell wall S2 layer. Scale bar: 5 μm.

this region is necessary for correct functioning of this structure. The super-resolution images were obtained by using Airyscan technology to analyze the results of triple labeling experiments on flax xylem cells (Figure 4). We stress here that this enables relative quantifications of fluorescence intensity within a single channel and comparisons of profiles between channels, but like in all fluorescence microscopy experiments, direct comparisons of fluorescence intensity between channels are not possible. Our results indicated that all three monolignol reporters were incorporated into the walls of the adjacent fiber-tracheids analyzed, thereby confirming their capacity to undergo lignification.

The data also reveal clear differences between the level of incorporation of the three monolignol units in the cell wall region immediately adjacent to the pit cavity (region R1) compared to either the neighboring region R2, or the regions R3 and R4 distant from the bordered pit. Indeed, three-dimensional surface maps of the fluorescence intensities corresponding to each individual reporter (Figure 4, panel B) reveal that the relative incorporation of H_{AZ} reporters is much higher in R1 compared to R2, while the relative incorporation of G_{ALK} reporters is similar in the two regions. In contrast, S_{CP} incorporation is lower in R1 compared to R2. The high relative incorporation of H_{AZ} and G_{ALK} reporters compared to S_{CP} in the pit border region compared to other wall regions of the same cell type was also confirmed by the individual intensity profiles P1−P3 of the three reporters (Figure 4, panel C). Taken together, these results clearly indicate that the pattern of monolignol reporter incorporation in the cell wall region immediately adjacent to the pit (R1) is very different from that of the immediately adjacent region (R2) which most closely resembles the incorporation pattern observed in the R3 region. Lignin containing high amounts of H-units is known to be more condensed than G-/S-rich lignin due to the absence of methoxy groups on the aromatic cycle favorizing the formation of condensed C−C bonds during polymerization.[49] The presence of a more resistant lignin in the cell wall immediately adjacent to the discontinuity would

https://doi.org/10.1021/cbmi.3c00052
Chem. Biomed. Imaging 2023, 1, 479−487

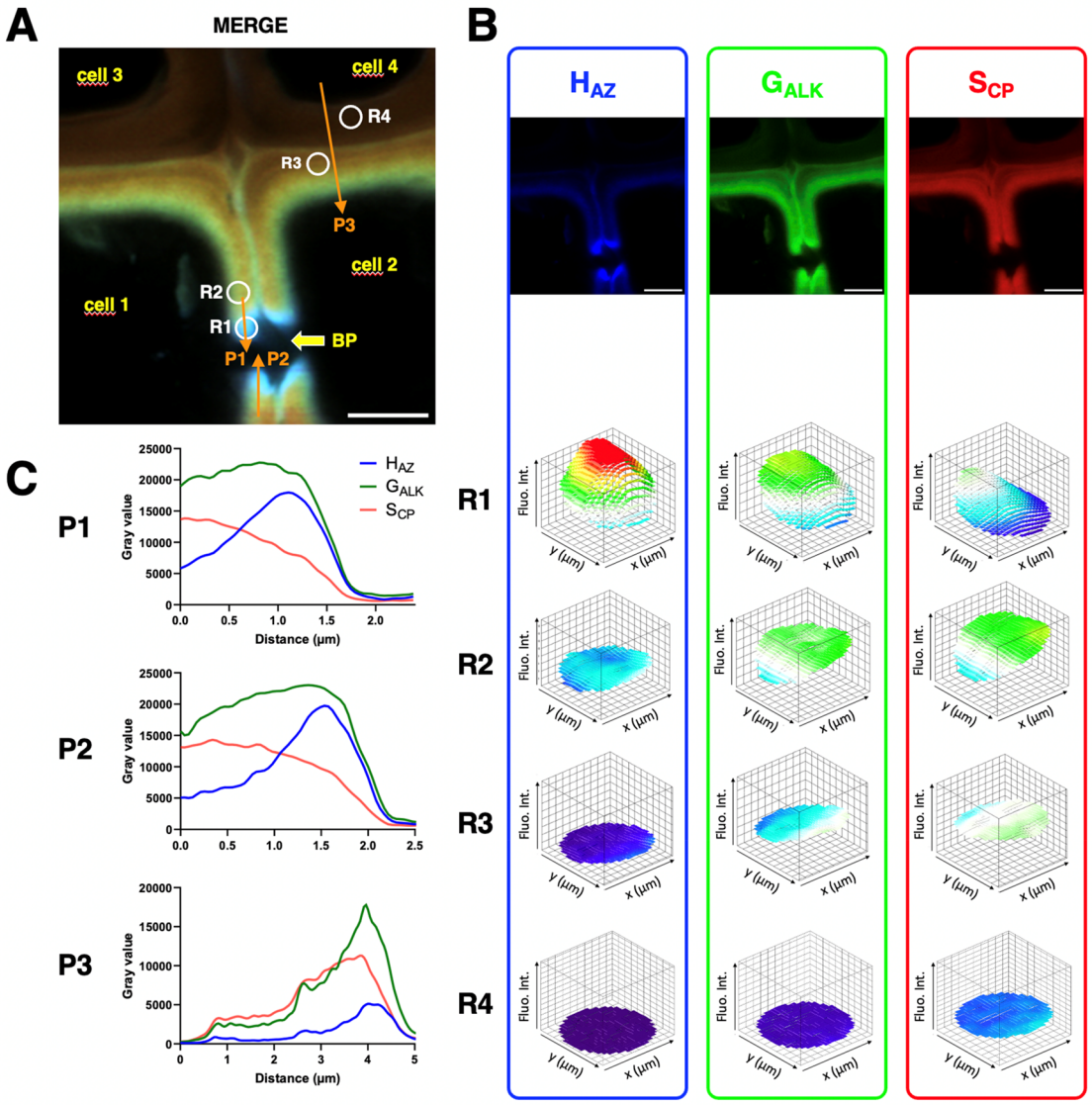

Figure 4. Analysis of monolignol reporter fluorescence in flax xylem pit border regions. (A) Airyscan merged image showing cell walls and a bordered pit (BP) between two cells in flax xylem; white circles R1−R4 show regions selected for 3D surface plots of different individual reporter (H_{AZ}, G_{ALK}, S_{CP}) fluorescence intensities, R1 and R2 = adjacent pit regions, R3 and R4 = two other cell wall regions for comparison; orange lines P1−P3 show vector lines used to trace individual reporter (H_{AZ}, G_{ALK}, S_{CP}) fluorescence intensity profiles along the lines. Scale bar = 3 μm. (B) 3D surface plots of different individual reporter (H_{AZ}, G_{ALK}, S_{CP}) fluorescence intensities. Signal intensity is indicated by *Z*-axis height and color: low (blue), medium (white to green), and high (yellow to red). (C) Individual reporter (H_{AZ}, G_{ALK}, S_{CP}) fluorescence intensity profiles for border pit profiles P1, P2, and P3. Note: fluorescence intensities can be compared between 2 coordinates within the same channel, but fluorescence intensities cannot be compared between channels.

certainly make sense from a mechanical point of view. Pits are also known to represent a potential entry point for vascular pathogens and a lignin more resistant to microbial enzymatic degradation could also contribute to reducing pathogen progress.[46]

Finally, it is also interesting to observe that the incorporation of all three reporters is low in the R4 region, indicating that the lignification process is almost completely terminated in the wall of this now mature xylem cell.

Monolignol triple-labeling and Airyscan super-resolution was also used to examine the lignification process in pits present between individual cells of *Arabidopsis* stem interfascicular fibers (Figures 5 and S1). In this case, the high-resolution images obtained using Airyscan technology allowed us to focus on the so-called "pit membrane". This structure, despite its name, is not composed of a phospholipid bilayer, but instead corresponds to a region of the cell wall in continuity with the middle lamella. Previous analyses of pit membrane composition have reported the presence of different polymers depending upon the technique used. Immunological approaches have indicated the presence of cellulose, lignin and pectins, but not hemicellulose.[47,50] Another study of pit membranes in *Populus nigra* xylem using synchrotron infrared nanospectroscopy (SINS) and atomic force microscopy-infrared nanospectroscopy (AFM-IR) revealed the presence of peaks related to lignin, cellulose and proteins.[51] Following triple-click lignin labeling in *A. thaliana* stems, we examined the relative intensity profiles of individual reporters in Airyscan data in the pit membranes of the pits from fiber cells. Since our approach detects active lignifying zones and their capacity to

https://doi.org/10.1021/cbmi.3c00052
Chem. Biomed. Imaging 2023, 1, 479−487

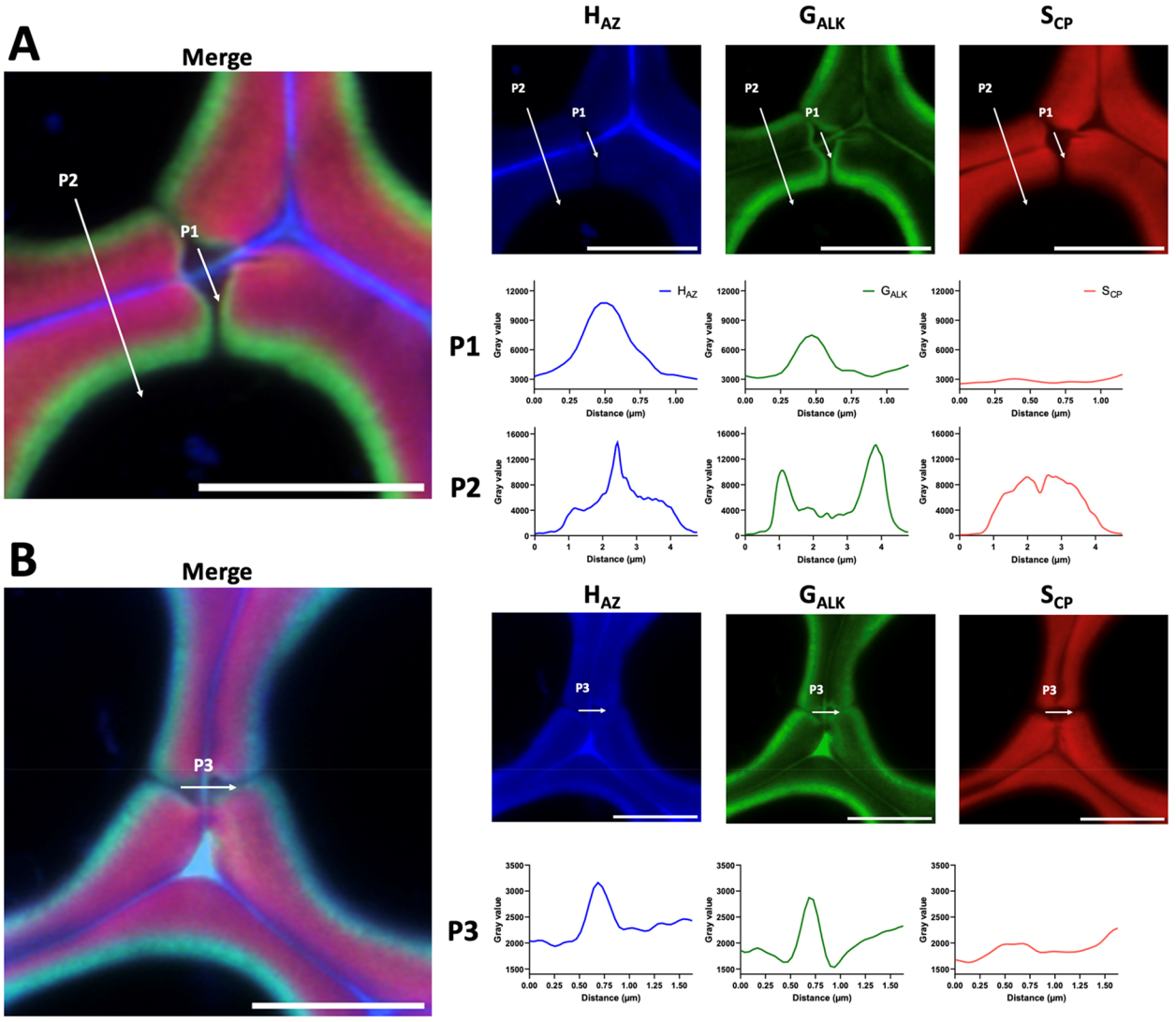

Figure 5. Analysis of monolignol reporter fluorescence in *Arabidopsis* interfascicular fiber pit membranes. (A,B) Airyscan single channel images together with corresponding probe intensity profiles and merged channel image. (A) Fiber pit membrane example 1 (profile arrow 1) and adjacent fiber wall (profile arrow 2); (B) fiber pit membrane example 2 (profile arrow 3). White arrow indicates intensity profile vector, scale bar = 5 μm.

differentially incorporate the three monolignol units, our results suggest that the lignin composition in the pit membranes (profiles 1 and 3) is different from that of the adjacent zones of the fiber cell walls (Figure 5). In both profiles P1 and P3 crossing pit membranes, S_{CP} reporter incorporation was homogeneous across the width and essentially nonsignificant when compared to the signal of S_{CP} in the secondary cell wall layers of the adjacent zone, which displayed a high level of incorporation (profile P2). In contrast, the signals corresponding to H_{AZ} and G_{ALK} incorporation are not homogeneous across the pit membrane, as they exhibit a maximum in profiles P1 and P3. Relatively, H_{AZ} is incorporated in higher proportions into the pit membranes (profiles P1 and P3) and middle lamellae (profile P2) when compared to the secondary cell wall, whereas G_{ALK} is significantly more integrated into lignin in the younger zones of the secondary cell wall than in any other substructure. Despite the apparent continuity of the pit membrane and middle lamella, the intensity profiles of these two contiguous regions, therefore, show important differences in reporter incorporation. Taken together, these results would suggest that the regulation of the lignification process is different in these two spatially close cell wall regions. Interestingly, differences in the lignin composition in G and S units (condensed vs noncondensed) of these two contiguous layers in tissues of another species, namely *Populus tremula* (Aspen trees) were also previously observed using an immunocytochemical approach.[50]

■ CONCLUSION

The combination of multiplexed bioorthogonal chemistry and Airyscan microscopy constitutes a powerful duo for investigating monolignol polymerization into substructures of plant cell walls. Airyscan offers a higher resolution than LSCM but is as easy to use, allowing a finer visualization of the dynamics of lignification in the different sublayers of the same cell wall. In addition, training and adapting the AI algorithm of the ratiometric REPRISAL technique that we have recently developed[21] with larger Airyscan data sets will allow a wide range of samples to be analyzed in the future. This will enable researchers to obtain statistically robust quantitative data on relative reporter incorporation in different cell wall layers and zones (such as pits illustrated in this work), thereby improving

https://doi.org/10.1021/cbmi.3c00052
Chem. Biomed. Imaging 2023, 1, 479−487

the quality of the biological information obtained. Other techniques like Raman spectroscopy or atomic force microscopy provide information on lignin microdomains in cell walls,[52] but not on the microdomains that are actively biosynthesizing lignin and their differential capacity to incorporate H, G, or S monolignols, contrary to the presented strategy. Since the triple-labeling strategy can also be exploited to analyze sugar incorporation into polysaccharides, this approach could also be used in the future to finely image the formation *in situ* of other plant cell wall polymers.[26]

■ ASSOCIATED CONTENT

Supporting Information

The Supporting Information is available free of charge at https://pubs.acs.org/doi/10.1021/cbmi.3c00052.

Synthesis and analytical data of chemical reporters, procedure for triple bioorthogonal lignin metabolic labeling (PDF)

■ AUTHOR INFORMATION

Corresponding Author

Cédric Lion − *Univ. Lille, CNRS, UMR 8576 - UGSF - Unité de Glycobiologie Structurale et Fonctionnelle, Lille 59655, France;* orcid.org/0000-0001-6591-4573; Email: cedric.lion@univ-lille.fr

Authors

Clémence Simon − *Univ. Lille, CNRS, UMR 8576 - UGSF - Unité de Glycobiologie Structurale et Fonctionnelle, Lille 59655, France*

Oriane Morel − *Univ. Lille, CNRS, UMR 8576 - UGSF - Unité de Glycobiologie Structurale et Fonctionnelle, Lille 59655, France*

Godfrey Neutelings − *Univ. Lille, CNRS, UMR 8576 - UGSF - Unité de Glycobiologie Structurale et Fonctionnelle, Lille 59655, France*

Fabien Baldacci-Cresp − *Univ. Lille, CNRS, UMR 8576 - UGSF - Unité de Glycobiologie Structurale et Fonctionnelle, Lille 59655, France*

Marie Baucher − *Laboratoire de Biotechnologie Végétale (LBV), Univ. Bruxelles, B-6041 Gosselies, Belgium*

Corentin Spriet − *Univ. Lille, CNRS, UMR 8576 - UGSF - Unité de Glycobiologie Structurale et Fonctionnelle, Lille 59655, France; Univ. Lille, CNRS, Inserm, CHU Lille, Institut Pasteur de Lille, US 41 - UMS 2014 - PLBS, Lille 59655, France;* orcid.org/0000-0002-5805-3426

Christophe Biot − *Univ. Lille, CNRS, UMR 8576 - UGSF - Unité de Glycobiologie Structurale et Fonctionnelle, Lille 59655, France;* orcid.org/0000-0002-7396-1959

Simon Hawkins − *Univ. Lille, CNRS, UMR 8576 - UGSF - Unité de Glycobiologie Structurale et Fonctionnelle, Lille 59655, France*

Complete contact information is available at: https://pubs.acs.org/10.1021/cbmi.3c00052

Notes

The authors declare no competing financial interest.

■ ACKNOWLEDGMENTS

We thank the TisBio facilities and the FRABio research federation for providing the technical environment conducive to achieving this work. This work was supported by grants from the Ministère de l'Enseignement Supérieur, de la Recherche et de l'Innovation and by the Human Frontier Science Program (LT000552/2020-L) to C.S.

■ REFERENCES

(1) Sletten, E. M.; Bertozzi, C. R. Bioorthogonal Chemistry: Fishing for Selectivity in a Sea of Functionality. *Angew. Chem., Int. Ed.* **2009**, *48* (38), 6974−6998.

(2) Scinto, S. L.; Bilodeau, D. A.; Hincapie, R.; Lee, W.; Nguyen, S. S.; Xu, M.; am Ende, C. W.; Finn, M. G.; Lang, K.; Lin, Q.; Pezacki, J. P.; Prescher, J. A.; Robillard, M. S.; Fox, J. M. Bioorthogonal Chemistry. *Nat. Rev. Methods Primers* **2021**, *1* (1), 1−23.

(3) Kolb, H. C.; Finn, M. G.; Sharpless, K. B. Click Chemistry: Diverse Chemical Function from a Few Good Reactions. *Angew. Chem., Int. Ed.* **2001**, *40* (11), 2004−2021.

(4) Bertozzi, C. R. A Decade of Bioorthogonal Chemistry. *Acc. Chem. Res.* **2011**, *44* (9), 651−653.

(5) Besanceney-Webler, C.; Jiang, H.; Zheng, T.; Feng, L.; Soriano del Amo, D.; Wang, W.; Klivansky, L. M.; Marlow, F. L.; Liu, Y.; Wu, P. Increasing the Efficacy of Bioorthogonal Click Reactions for Bioconjugation: A Comparative Study. *Angew. Chem., Int. Ed.* **2011**, *50* (35), 8051−8056.

(6) Patterson, D. M.; Nazarova, L. A.; Xie, B.; Kamber, D. N.; Prescher, J. A. Functionalized Cyclopropenes As Bioorthogonal Chemical Reporters. *J. Am. Chem. Soc.* **2012**, *134* (45), 18638−18643.

(7) Rigolot, V.; Biot, C.; Lion, C. To View Your Biomolecule, Click inside the Cell. *Angew. Chem., Int. Ed.* **2021**, *60* (43), 23084−23105.

(8) Kufleitner, M.; Haiber, L. M.; Wittmann, V. Metabolic Glycoengineering − Exploring Glycosylation with Bioorthogonal Chemistry. *Chem. Soc. Rev.* **2023**, *52* (2), 510−535.

(9) Banahene, N.; Kavunja, H. W.; Swarts, B. M. Chemical Reporters for Bacterial Glycans: Development and Applications. *Chem. Rev.* **2022**, *122* (3), 3336−3413.

(10) Chiu, D.-C.; Baskin, J. M. Imaging and Editing the Phospholipidome. *Acc. Chem. Res.* **2022**, *55* (21), 3088−3098.

(11) Müggenburg, F.; Müller, S. Azide-Modified Nucleosides as Versatile Tools for Bioorthogonal Labeling and Functionalization. *Chem. Rec.* **2022**, *22* (5), No. e202100322.

(12) Lang, K.; Chin, J. W. Bioorthogonal Reactions for Labeling Proteins. *ACS Chem. Biol.* **2014**, *9* (1), 16−20.

(13) Lee, S.; Kim, J.; Koh, M. Recent Advances in Fluorescence Imaging by Genetically Encoded Non-Canonical Amino Acids. *J. Mol. Biol.* **2022**, *434* (8), No. 167248.

(14) Sletten, E. M.; Bertozzi, C. R. From Mechanism to Mouse: A Tale of Two Bioorthogonal Reactions. *Acc. Chem. Res.* **2011**, *44* (9), 666−676.

(15) Kenry; Liu, B. Bio-Orthogonal Click Chemistry for In Vivo Bioimaging. *Trends in Chemistry* **2019**, *1* (8), 763−778.

(16) Bukowski, N.; Pandey, J. L.; Doyle, L.; Richard, T. L.; Anderson, C. T.; Zhu, Y. Development of a Clickable Designer Monolignol for Interrogation of Lignification in Plant Cell Walls. *Bioconjugate Chem.* **2014**, *25* (12), 2189−2196.

(17) Tobimatsu, Y.; Van de Wouwer, D.; Allen, E.; Kumpf, R.; Vanholme, B.; Boerjan, W.; Ralph, J. A Click Chemistry Strategy for Visualization of Plant Cell Wall Lignification. *Chem. Commun.* **2014**, *50* (82), 12262−12265.

(18) (a) Dumont, M.; Lehner, A.; Vauzeilles, B.; Malassis, J.; Marchant, A.; Smyth, K.; Linclau, B.; Baron, A.; Pons, J. M.; Anderson, C. T.; Schapman, D.; Galas, L.; Mollet, J.-C.; Lerouge, P. Plant Cell Wall Imaging by Metabolic Click-Mediated Labelling of Rhamnogalacturonan II Using Azido 3-Deoxy-d-Manno-Oct-2-Ulosonic Acid. *Plant J.* **2016**, *85* (3), 437−447. (b) Ropitaux, M.; Hays, Q.; Baron, A.; Fourmois, L.; Boulogne, I.; Vauzeilles, B.; Lerouge, P.; Mollet, J.-C.; Lehner, A. Dynamic imaging of cell wall polysaccharides by metabolic click-mediated labeling of pectins in living elongating cells. *Plant J.* **2022**, *110* (3), 916−924.

(19) Glenn, W. S.; Stone, S. E.; Ho, S. H.; Sweredoski, M. J.; Moradian, A.; Hess, S.; Bailey-Serres, J.; Tirrell, D. A. Bioorthogonal Noncanonical Amino Acid Tagging (BONCAT) Enables Time-Resolved Analysis of Protein Synthesis in Native Plant Tissue. *Plant Physiol* **2017**, *173* (3), 1543−1553.
(20) Zhu, Y.; Chen, X. Expanding the Scope of Metabolic Glycan Labeling in Arabidopsis Thaliana. *Chembiochem* **2017**, *18* (13), 1286−1296.
(21) Morel, O.; Lion, C.; Neutelings, G.; Stefanov, J.; Baldacci-Cresp, F.; Simon, C.; Biot, C.; Hawkins, S.; Spriet, C. REPRISAL: Mapping Lignification Dynamics Using Chemistry, Data Segmentation, and Ratiometric Analysis. *Plant Physiol* **2022**, *188* (2), 816−830.
(22) Paper, J. M.; Mukherjee, T.; Schrick, K. Bioorthogonal Click Chemistry for Fluorescence Imaging of Choline Phospholipids in Plants. *Plant Methods* **2018**, *14* (1), 31.
(23) Vanholme, R.; Morreel, K.; Ralph, J.; Boerjan, W. Lignin Engineering. *Curr. Opin. Plant Biol.* **2008**, *11* (3), 278−285.
(24) Liu, Q.; Luo, L.; Zheng, L. Lignins: Biosynthesis and Biological Functions in Plants. *Int. J. Mol. Sci.* **2018**, *19* (2), 335.
(25) Lion, C.; Simon, C.; Huss, B.; Blervacq, A.-S.; Tirot, L.; Toybou, D.; Spriet, C.; Slomianny, C.; Guerardel, Y.; Hawkins, S.; Biot, C. BLISS: A Bioorthogonal Dual-Labeling Strategy to Unravel Lignification Dynamics in Plants. *Cell Chem. Biol.* **2017**, *24* (3), 326−338.
(26) Simon, C.; Lion, C.; Spriet, C.; Baldacci-Cresp, F.; Hawkins, S.; Biot, C. One, Two, Three: A Bioorthogonal Triple Labelling Strategy for Studying the Dynamics of Plant Cell Wall Formation In Vivo. *Angew. Chem., Int. Ed.* **2018**, *57* (51), 16665−16671.
(27) Conchello, J.-A.; Lichtman, J. W. Optical Sectioning Microscopy. *Nat. Methods* **2005**, *2* (12), 920−931.
(28) Klar, T. A.; Jakobs, S.; Dyba, M.; Egner, A.; Hell, S. W. Fluorescence Microscopy with Diffraction Resolution Barrier Broken by Stimulated Emission. *Proc. Natl. Acad. Sci. U. S. A.* **2000**, *97* (15), 8206−8210.
(29) Betzig, E.; Patterson, G. H.; Sougrat, R.; Lindwasser, O. W.; Olenych, S.; Bonifacino, J. S.; Davidson, M. W.; Lippincott-Schwartz, J.; Hess, H. F. Imaging Intracellular Fluorescent Proteins at Nanometer Resolution. *Science* **2006**, *313* (5793), 1642−1645.
(30) Hess, S. T.; Girirajan, T. P. K.; Mason, M. D. Ultra-High Resolution Imaging by Fluorescence Photoactivation Localization Microscopy. *Biophys. J.* **2006**, *91* (11), 4258−4272.
(31) Rust, M. J.; Bates, M.; Zhuang, X. Sub-Diffraction-Limit Imaging by Stochastic Optical Reconstruction Microscopy (STORM). *Nat. Methods* **2006**, *3* (10), 793−796.
(32) van de Linde, S.; Löschberger, A.; Klein, T.; Heidbreder, M.; Wolter, S.; Heilemann, M.; Sauer, M. Direct Stochastic Optical Reconstruction Microscopy with Standard Fluorescent Probes. *Nat. Protoc* **2011**, *6* (7), 991−1009.
(33) Vangindertael, J.; Camacho, R.; Sempels, W.; Mizuno, H.; Dedecker, P.; Janssen, K. P. F. An Introduction to Optical Super-Resolution Microscopy for the Adventurous Biologist. *Methods Appl. Fluoresc* **2018**, *6* (2), No. 022003.
(34) Vicidomini, G.; Bianchini, P.; Diaspro, A. STED Super-Resolved Microscopy. *Nat. Methods* **2018**, *15* (3), 173−182.
(35) Gustafsson, N.; Culley, S.; Ashdown, G.; Owen, D. M.; Pereira, P. M.; Henriques, R. Fast Live-Cell Conventional Fluorophore Nanoscopy with ImageJ through Super-Resolution Radial Fluctuations. *Nat. Commun.* **2016**, *7*, 12471.
(36) Korobchevskaya, K.; Lagerholm, B. C.; Colin-York, H.; Fritzsche, M. Exploring the Potential of Airyscan Microscopy for Live Cell Imaging. *Photonics* **2017**, *4* (3), 41.
(37) Scipioni, L.; Lanzanó, L.; Diaspro, A.; Gratton, E. Comprehensive Correlation Analysis for Super-Resolution Dynamic Fingerprinting of Cellular Compartments Using the Zeiss Airyscan Detector. *Nat. Commun.* **2018**, *9* (1), 5120.
(38) Komis, G.; Šamajová, O.; Ovečka, M.; Šamaj, J. Super-Resolution Microscopy in Plant Cell Imaging. *Trends Plant Sci.* **2015**, *20* (12), 834−843.
(39) Schubert, V. Super-Resolution Microscopy − Applications in Plant Cell Research. *Frontiers in Plant Science* **2017**, *8*, 531.
(40) Ovečka, M.; Sojka, J.; Tichá, M.; Komis, G.; Basheer, J.; Marchetti, C.; Šamajová, O.; Kuběnová, L.; Šamaj, J. Imaging Plant Cells and Organs with Light-Sheet and Super-Resolution Microscopy. *Plant Physiology* **2022**, *188* (2), 683−702.
(41) Liesche, J.; Ziomkiewicz, I.; Schulz, A. Super-Resolution Imaging with Pontamine Fast Scarlet 4BS Enables Direct Visualization of Cellulose Orientation and Cell Connection Architecture in Onion Epidermis Cells. *BMC Plant Biol.* **2013**, *13* (1), 226.
(42) Haas, K. T.; Wightman, R.; Meyerowitz, E. M.; Peaucelle, A. Pectin Homogalacturonan Nanofilament Expansion Drives Morphogenesis in Plant Epidermal Cells. *Science* **2020**, *367* (6481), 1003−1007.
(43) Paës, G.; Habrant, A.; Terryn, C. Fluorescent Nano-Probes to Image Plant Cell Walls by Super-Resolution STED Microscopy. *Plants* **2018**, *7* (1), 11.
(44) Donaldson, L. A. Super-Resolution Imaging of Douglas Fir Xylem Cell Wall Nanostructure Using SRRF Microscopy. *Plant Methods* **2022**, *18* (1), 27.
(45) Huff, J. The Airyscan Detector from ZEISS: Confocal Imaging with Improved Signal-to-Noise Ratio and Super-Resolution. *Nat. Methods* **2015**, *12*, 1205.
(46) Choat, B.; Cobb, A. R.; Jansen, S. Structure and Function of Bordered Pits: New Discoveries and Impacts on Whole-Plant Hydraulic Function. *New Phytologist* **2008**, *177* (3), 608−626.
(47) Fromm, J.; Rockel, B.; Lautner, S.; Windeisen, E.; Wanner, G. Lignin Distribution in Wood Cell Walls Determined by TEM and Backscattered SEM Techniques. *J. Struct. Biol.* **2003**, *143* (1), 77−84.
(48) Baldacci-Cresp, F.; Spriet, C.; Twyffels, L.; Blervacq, A.-S.; Neutelings, G.; Baucher, M.; Hawkins, S. A Rapid and Quantitative Safranin-Based Fluorescent Microscopy Method to Evaluate Cell Wall Lignification. *Plant J.* **2020**, *102* (5), 1074−1089.
(49) Terashima, N.; Fukushima, K. Heterogeneity in Formation of Lignin—XI: An Autoradiographic Study of the Heterogeneous Formation and Structure of Pine Lignin. *Wood Sci.Technol.* **1988**, *22* (3), 259−270.
(50) Herbette, S.; Bouchet, B.; Brunel, N.; Bonnin, E.; Cochard, H.; Guillon, F. Immunolabelling of Intervessel Pits for Polysaccharides and Lignin Helps in Understanding Their Hydraulic Properties in Populus Tremula × Alba. *Ann. Bot* **2015**, *115* (2), 187−199.
(51) Pereira, L.; Flores-Borges, D. N. A.; Bittencourt, P. R. L.; Mayer, J. L. S.; Kiyota, E.; Araújo, P.; Jansen, S.; Freitas, R. O.; Oliveira, R. S.; Mazzafera, P. Infrared Nanospectroscopy Reveals the Chemical Nature of Pit Membranes in Water-Conducting Cells of the Plant Xylem. *Plant Physiol.* **2018**, *177* (4), 1629−1638.
(52) Farahi, R. H.; Charrier, A. M.; Tolbert, A.; Lereu, A. L.; Ragauskas, A.; Davison, B. H.; Passian, A. Plasticity, Elasticity, and Adhesion Energy of Plant Cell Walls: Nanometrology of Lignin Loss Using Atomic Force Microscopy. *Sci. Rep* **2017**, *7* (1), 152.

https://doi.org/10.1021/cbmi.3c00052
Chem. Biomed. Imaging 2023, 1, 479−487